Regulatory Mechanisms in Biosystems

ISSN 2519-8521 (Print)
ISSN 2520-2588 (Online)
Regul. Mech. Biosyst.

Synthesis of a kinetin and graphene oxide nanoensemble and its effects on defense responses of cotton against *Verticillium dahliae*

N. R. Amrahov*, U. A. Hasanova*, M. Levy**, G. S. Aliyeva*, G. A. Aghazada*, R. B. Mammadova***, S. A. Alizade***, F. H. Rzayev****, E. K. Gasimov****, S. S. Hasanova*, N. A. Malikova*, Z. M. Mammadov*

**Baku State University, Baku, Azerbaijan*
*** The Hebrew University of Jerusalem, Rehovot, Israel*
**** Genetic Resources Institute, Ministry of Science and Education of the Republic of Azerbaijan, Baku, Azerbaijan*
***** Azerbaijan Medical University, Baku, Azerbaijan*

Article info
Received 14.03.2026
Received in revised form 07.05.2026
Accepted 25.05.2026

Baku State University, Academic Zahid Khalilov st., 33, Baku, AZ1148, Azerbaijan. Tel.: +994-12-430-32-45. E-mail:nurlanamrahov@bsu.edu.az

Department of Plant Pathology and Microbiology, The Robert H. Smith Faculty of Agriculture, Food and Environment, The Hebrew University of Jerusalem, Rehovot, 76100, Israel. Tel.: +972-894-891-60. E-mail: maggie.levy@mail.huji.ac.il

Genetic Resources Institute, Ministry of Science and Education Republic of Azerbaijan, Azadlig av., 155, Baku, AZ1106, Azerbaijan. Tel.: +994-12-449-92-21. E-mail: gene-res@mail.ru

Azerbaijan Medical University, Ministry of Science and Education of the Republic of Azerbaijan, Samad Vurgun st., 163, Baku, AZ1078, Azerbaijan. E-mail: fuad.rzayev@amu.edu.az

Amrahov, N. R., Hasanova, U. A., Levy, M., Aliyeva, G. S., Aghazada, G. A., Mammadova, R. B., Alizade, S. A., Rzayev, F. H., Gasimov, E. K., Hasanova, S. S., Malikova, N. A., & Mammadov, Z. M. (2026). Synthesis of a kinetin and graphene oxide nanoensemble and its effects on defense responses of cotton against Verticillium dahliae. Regulatory Mechanisms in Biosystems, 17(4), e26077. doi:10.15421/0226077

In this study, a kinetin-graphene oxide nanoensemble (KN+GO) was synthesized via non-covalent interactions. Its structure and morphology were characterized by transmission electron microscopy (TEM), Fourier transform infrared (FTIR) spectroscopy, and powder X-ray diffraction (XRD), confirming the successful immobilization of kinetin on graphene oxide. The loading efficiency of kinetin on GO was determined by UV–Vis spectroscopy. The effects of the KN+GO nanoensemble on the physiological and biochemical responses of two cotton genotypes (*Gossypium hirsutum* L. TM-1 and *G. barbadense* L. Pima 3-79) were investigated during infection with *Verticillium dahliae*. Morphometric traits, seedling survival, antioxidant enzyme activities (catalase, peroxidase, and polyphenol oxidase), nitric oxide and proline levels, and photosynthetic pigment composition were analyzed. Pathogen infection induced oxidative stress and significantly altered the growth and biochemical parameters in both genotypes. Free kinetin exhibited genotype-dependent effects, whereas the KN+GO nanoensemble consistently enhanced stress tolerance, particularly under pathogen pressure. In the TM-1 plants, KN+GO markedly improved seedling survival, increased antioxidant enzyme activity, promoted proline accumulation, and stabilized photosynthetic pigment levels. In the Pima 3-79 plants, the nanoensemble mainly supported survival and redox balance, although the responses were less pronounced. These findings demonstrate that graphene oxide–based kinetin nanoensembles modulate cotton defense responses in a genotype- and stress-dependent manner, highlighting their potential as nano-enabled phytohormone delivery systems for improving resistance to fungal pathogens.

Keywords: phytohormone delivery; carbon nanomaterials; plant–pathogen interaction; *Verticillium dahliae*; cotton genotypes; non-covalent functionalization.

Introduction

Cotton (*Gossypium* spp.) is one of the most economically and strategically significant crops, serving as an essential source of fiber and oilseed. It is one of the most important crops in Azerbaijan, playing a significant role in the country's agricultural production and export economy (Mammadova et al., 2025).

Yield and fiber quality of cotton remain significantly constrained by biotic stress factors, among which the fungal pathogen *Verticillium dahliae* Kleb. plays a major role (Alizada et al,. 2024). This causal agent of *Verticillium* wilt infects root systems and vascular tissues and can persist in the soil for extended periods, causing considerable yield losses (Zhu et al,. 2023).

The negative impact of *V. dahliae* is manifested through disruption of water and mineral uptake, reduced cell turgor, and osmotic imbalance, ultimately decreasing the overall stress tolerance of the plants. Therefore, the development of effective strategies to enhance plant resistance to pathogens, including the use of natural and synthetic inducers of plant defense, is an urgent research priority.

One promising approach involves the application of phytohormones and their derivatives, which can induce innate plant defense mechanisms (Di et al., 2016). Cytokinins, particularly kinetin (6-furfurylaminopurine), are known to regulate cell division, morphogenesis, and the activation of antioxidant systems, as well as to participate in the modulation of both primary and secondary defense responses (PTI and ETI). Kinetin enhances the expression of PR genes, responsible for ETI, and activates systemic acquired resistance (SAR) in coordination with salicylic acid (Choi et al., 2011). Through coordinated hormonal signaling, kinetin can act as an inducer of defense responses against both pathogens and abiotic stressors (Chun et al., 2024).

Recent advances in nanobiotechnology have promoted the development of carbon-based nanomaterials as promising carriers for phytohormones and other bioactive compounds (Chen et al., 2014). For example, graphene oxide (GO) enhances the stability, bioavailability, and targeted delivery of growth regulators due to its large surface area, oxygen-containing functional groups, and biocompatibility. Studies have shown that GO not only serves as an effective carrier, enabling controlled release of active molecules, but also acts as an independent modulator of cellular defense mechanisms (Kabiri et al., 2017; Park et al., 2020).

The combination of GO with kinetin may amplify the physiological and protective effects of the hormone, forming a synergistic nanoensemble capable of activating stress-responsive regulatory pathways in plants. Despite growing interest in cytokinins and nanomaterials that have been studied separately, information on their synergistic effects on the infected cotton genotypes remains limited.

The objective of the present study was to analyze the physiological and biochemical responses of two cotton genotypes (*G. hirsutum* L. TM-1 and *G. barbadense* L. Pima 3-79) to kinetin and KN+GO nanoensemble during infection with *Verticillium dahliae*. The research was focused on morphometric parameters, antioxidant enzyme activities, levels of signaling molecules (NO and proline), and the pigment composition of the photosynthetic apparatus, providing insights into the potential of the KN+GO for enhancing plant defense capacity.

Materials and methods

The chemicals were obtained from Sigma-Aldrich (St. Louis, MO, USA) and employed without further purification steps. All experiments were conducted at least twice to ensure reproducibility.

Graphene oxide (GO) nanolayers were prepared using a modified Hummers method (Taghiyeva et al., 2024). For the synthesis of the KN+GO nanoensemble, the dispersion of GO (0.05 g) in 10 mL of glacial acetic acid was subjected to ultrasonication for 15 min. Subsequently, a kinetin solution (0.2 g in 20 mL glacial acetic acid) was gradually introduced into the GO dispersion under continuous stirring, and the reaction mixture was then maintained under constant stirring for 24 h. The obtained solid product was collected by filtration, sequentially washed with acetic acid and distilled water, and dried at room temperature.

We prepared KN+GO nanoensemle by non-covalent functionalization of GO with kinetin molecules. Kinetin is a phytohormone promoting growth-related reactions in plant cells. This nanoensemble has been designed to provide a more efficient transport of kinetin into plant cells. We intentionally performed non-covalent functionalization of GO with kinetin, as biomaterials in natural biological environments are designed to remain stable over typical biological timescales. They are designed to perform a specific task and then readily degrade, providing a nontoxic starting material. They are stable at biological temperatures, but not too stable, allowing for rapid assembly or disassembly within seconds. The scheme below presents the hydrogen bonds occurring when oxygen containing groups of GO interact with N-H and C=N functional groups of kinetin (Fig. 1).

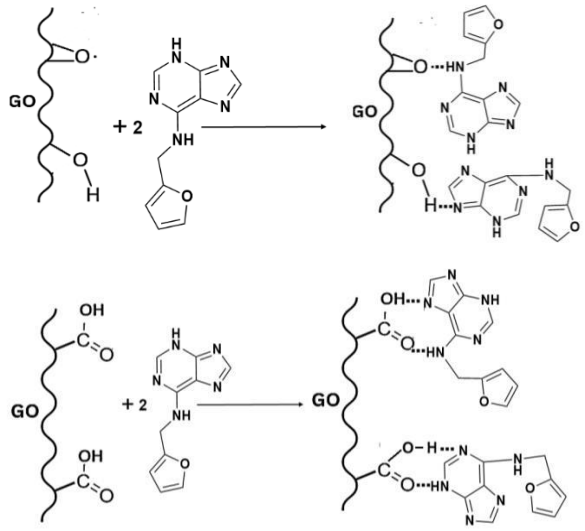

Fig. 1. Scheme of interactions between GO and kinetin

The loading of kinetin on the GO was determined using the spectrophotometric method. The UV–Vis spectrum of kinetin was recorded using a Jenway 6850 spectrophotometer at 264 nm (Bibby Scientific Ltd., Staffordshire, UK).

The concentration was determined using a calibration curve based on the Beer-Lambert law. Standard kinetin solutions with concentrations ranging from 10 to 60 ppm were prepared and analyzed at λ_{max} = 264 nm. The obtained values were used to construct a linear calibration curve and to calculate the amount of loaded kinetin. The loading efficiency was determined to be 99.4% (Fig. 2).

KN+GO nanoensembles were analyzed using a Fourier transform infrared spectrometer (FTIR) Nicolet iS50 (Thermo Scientific, Waltham, MA, USA), equipped with an attenuated total reflectance (ATR) attachment, in the range of 4,000–450 cm^{-1}.

The FTIR spectra of the prepared nanostructures and pure kinetin are presented in Figure 3, evidencing hydrogen bonds and π–π interactions between GO and kinetin. A broad and relatively weak-to-moderate intensity band is observed in the GO spectrum in the region of 3,200–3,600 cm^{-1} (Fig. 3). This band is responsible for the vibrations of hydroxyl (–OH) and adsorbed water molecules on the surface. The width of the band indicates the presence of numerous hydroxy functional groups on GO and the interaction with water (Fatehi et al., 2022). A sharper and more well-defined band or peak can also be seen in the kinetin spectrum around 3,300–3,400 cm^{-1}; this is indicative of NH or NH-type functionalities (H attached to purine nitrogen) or heterocyclic hydrogenatable sites in the kinetin molecule (Barnaby et al., 2011). In the composite spectrum, the O–H/N–H band fluctuates and often shifts. In particular, this band is broader or slightly shifted compared with the GO spectrum, indicating the presence of strong hydrogen bonds (H-bonds) or proton transfer between kinetin and GO. As a result of the formation of hydrogen bonds, the band is usually slightly shifted to the right (lower wave number). One of the most characteristic bands for GO is the conventional carbonyl/carboxyl peak in the region of ~1,700–1,740 cm^{-1} (C=O). This band confirms the presence of carboxyl and carbonyl groups, which are oxidation products of GO. In addition, in the region of 1,600–1,620 cm^{-1}, graphitic C=C (aromatic/carbon skeleton) or water-related vibrations appear (Kalidas et al., 2024; Taghiyeva et al., 2024). In kinetin, the C=N and aromatic system vibrations are observed in the region of 1,500–1,650 cm^{-1}. These bands are interpreted as characteristic C=N and heteroaromatic signals for kinetin. In KN+GO, the C=O intensity of GO around ~1,700 cm^{-1} is weakened and this peak is slightly shifted, which may be attributed to the adsorption of kinetin on the GO surface and sharing hydrogen bonds or electron density with carboxyl and carbonyl groups. Also, additional or enhanced signals are seen at the points of the C=N/C=C bands of kinetin, which indicates the chemical-physical binding of kinetin to the GO surface. The decrease in the GO carbonyl band may also be an indicator of a partial reduction (reduction-like) process – that is, kinetin may have reduced or passivated some oxygen groups of GO as a result of their interaction. The region 1,220–1,050 cm^{-1} represents the C–O (epoxide/alkoxyl) vibrations for GO, and these bands are broad and clear in GO. These peaks indicate the rich oxygen functionalities and epoxide groups of GO. In the spectrum of kinetin, several peaks appear between 1,200–1,000 cm^{-1}, corresponding to the furan-oxo group and heterocyclic C–O/C–N representatives. In addition, C–O and ring vibrations specific to kinetin are present in this region. In the KN+GO, an overlap of peaks specific to both GO and kinetin is observed in this region; however, changes in the intensity of the peaks (some weakening, while others appear as new or broadened ones) indicate that kinetin binds to GO epoxide/alkoxyl groups through hydrogen bonds or π–π interactions.

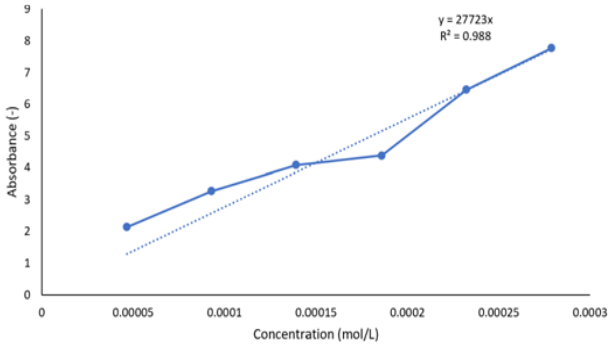

Fig. 2. Calibration curve of kinetin

Morphological analysis of the samples (GO and KN+GO nanoensembles) was performed using a high-resolution JEM-1400 transmission electron microscope (Jeol Ltd., Tokyo, Japan) equipped with a LaB4 electron gun and operating at an accelerating voltage of 80-120 kV. The samples were prepared by dispersing the sample material in water in an appropriate solvent using ultrasound for 15 minutes to obtain a homogeneous suspension. A few microliters of the suspension were dropped onto a carbon-coated copper grid (200 mesh, EMS, USA) and left to dry in ambient conditions. The TEM was operated in bright-field mode to capture high-contrast images of the microstructure. The magnification range used varied from 10.000x to 100.000x depending on the size of the feature of interest (Hajiyeva et al., 2019; Ahmadov et al., 2020).

During TEM analysis, graphene oxide nanomaterials are typically observed as thin, transparent, and layered structures. Since GO is mainly an oxidized form of graphene sheets, both amorphous and semicrystalline regions are visible in the layers. In electron microscopy images, certain wrinkles and folds can be observed on the surface of GO, which are due to its flexibility and bendability (Fig. 4a) (Baghirov et al., 2023; Huseynzada et al., 2023). Single layers have a much lighter and transparent contrast, while multilayers have a darker contrast, allowing us to visually determine their thickness differences. The TEM analysis of the samples revealed that the KN+GO sample exhibited a different morphology compared with GO. First, the layers aggregated more because of the binding of kinetin to the GO surface. This is characterized by increased aggregation and overlapping of the layers, which affects the contrast in TEM images rather than indicating a reduction in the interlayer spacing. As a result, KN+GO structures appear as darker, thicker layers in TEM images. In addition, the local accumulation of kinetin molecules on the GO surface is observed with a grain-like contrast change in certain regions. This is reflected as dotted black spots on the GO surface (Fig. 4b). These changes indicate the successful grafting of kinetin molecules on the GO surface to form the stable nanoconjugate.

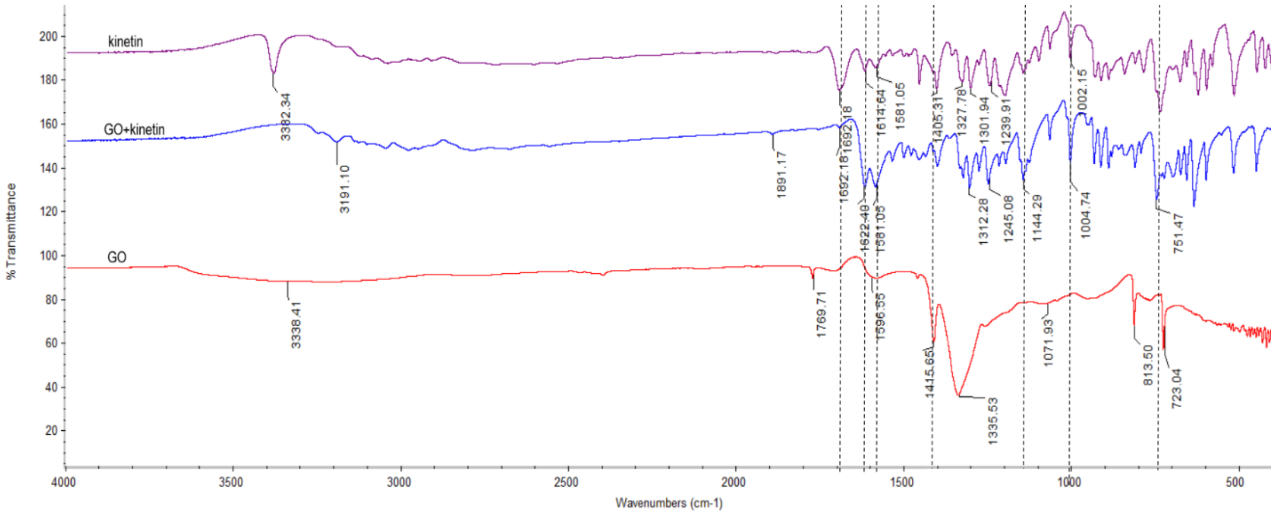

Fig. 3. FTIR spectra of GO, kinetin and KN+GO nanoensemble

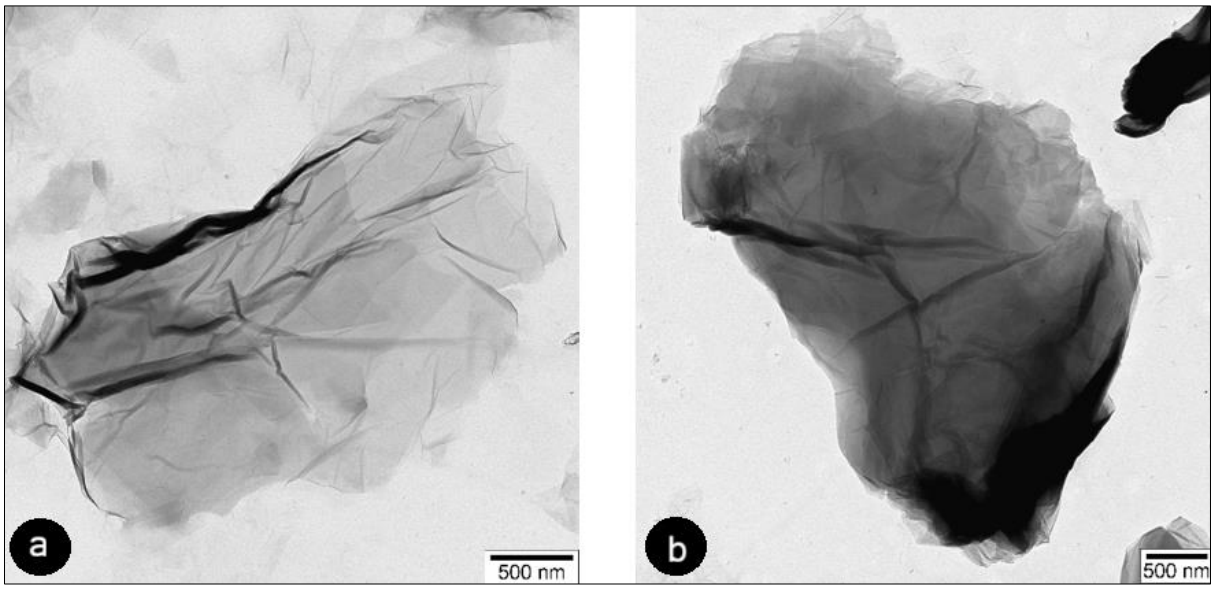

Fig. 4. TEM images of GO (*a*) and KN+GO nanoensemble (*b*)

X-ray diffraction (XRD) patterns of powder samples were obtained using a Bruker D2 PHASER diffractometer (Bruker AXS GmbH, Karlsruhe, Germany) operating at 30 kV and 10 mA with CuKα radiation. The diffraction patterns were recorded over a 2θ range of 5–80°. (Hajiyeva et al., 2019).

The diffractogram of the obtained graphene oxide (GO) (Fig. 5a) is characterized by the appearance of the main diffraction peak in the region of 2θ = 11.30°, corresponding to the (001) plane. This peak reflects the increased interlayer distance resulting from the extensive functionalization of the surface by oxygen-containing groups (–OH, –COOH, C–O–C). The interlayer distance equal to d = 0.787 nm, calculated using Bragg's equation, corresponds to the typical structural features of graphene oxide, confirming the successful oxidation and flaking of graphite (Hidayah et al., 2017): $\lambda = 2d\sin\theta$ (Magro et al., 2025).

After modification of graphene oxide with kinetin (Fig. 5b), the shifting of the main diffraction peak of graphene oxide from 2θ = 11.30° to 9.08° was observed, as well as an increase in the interlayer distance from d = 0.787 nm to d = 0.973 nm. Such a shift to the area of smaller angles clearly indicates the intercalation of molecules between the graphene oxide's sheets. The introduction of kinetin's fragments increases the distance between GO plates, leading to changes in the initial crystalline structure of kinetin (Fig. 5c). Comparing the XRD patterns of modified and unmodified GO, we observed a change in morphology, indicating successful GO modification, resulting in the formation of a stable hybrid nanocomposite system. This structural organization is highly advantageous for sustained release, as the layered GO structure can effectively adsorb and gradually release kinetin molecules over time.

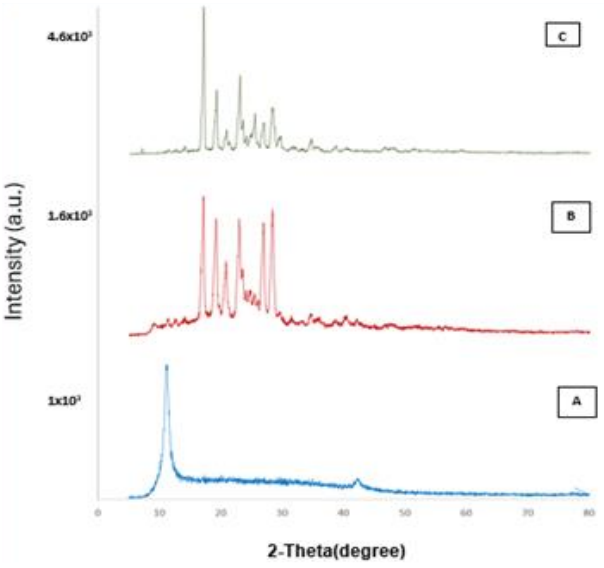

Fig. 5. The XRD pattern of GO (*a*), KN+GO (*b*) and Kinetin (*c*)

Preparation phase experiments were conducted using two cotton species: Egyptian cotton (*Gossypium barbadense* L., cv. Pima 3-79) and upland cotton (*Gossypium hirsutum* L., cv. TM-1).

Seeds were surface-sterilized in 0.3% potassium permanganate solution for 5 min and subsequently sown in 7 cm plastic containers filled with a soil mixture consisting of soil, perlite, and sand in a 3:1:1 ratio.

The seedlings were cultivated in a phytotron Taisite GZX-300 E (Taisite Instrument Co., Tianjin, China) under controlled conditions: 24–26 °C temperature, 65–75% relative humidity, and 4,800 lux light intensity, with a 14/10 h light/dark photoperiod.

Hoagland nutrient solution was used as the growth medium. In separate experiments, the plants were treated with either kinetin or the KN+GO nanoensemble by adding the respective compound to the Hoagland nutrient solution after seed sowing (Fig. 6).

Kinetin (10 µM) and KN+GO (equivalent to 10 µM kinetin) were applied throughout the entire growth period, starting from the early stages of seedling development. Prior to application, both compounds were dissolved in 10 mL of 96% ethanol, followed by ultrasonication, and then added to the hydroponic solution.

The *V. dahliae* VD-11 strain was obtained from the infected cotton plants according to Göre (2007). The inoculum was prepared by culturing the fungus on potato dextrose agar (PDA) plates at 24 °C. Two weeks later, conidia were harvested, suspended in sterile water, and maintained on PDA at 26 °C. Spore concentration was determined using a hemocytometer and adjusted to 2×10^7 conidia/mL for subsequent inoculation (Joost et al., 1995).

To establish fungal infection under hydroponic conditions, the conidial suspension was introduced directly into the Hoagland nutrient solution at a rate of 5 ml per 1 L of nutrient medium. Inoculation, together with the application of phytohormones and their graphene oxide nanoensembles, was performed at the beginning of the experiment simultaneously with seed sowing, allowing continuous exposure of the developing root system to the pathogen throughout the cultivation period. Control plants were grown under identical conditions without the addition of the fungal suspension.

As phytohormones, kinetin was used at the minimum activating concentration of 10 µM, in both pure kinetin and KN+GO.

Survival parameters of seedlings were evaluated based on the number of viable plants in each experimental variant. In the three biological replications, 30 seeds per treatment were used. The survival percentage was calculated using the following formula:

Survival (%) = (number of surviving plants / total number of planted seeds) × 100

Morphometric traits, including stem length and root length, were determined in randomly selected seedlings from each experimental group (n = 10). Stem length was measured as the distance from the cotyledonary node to the shoot apical meristem, whereas root length was measured from the root collar to the tip of the primary root. Measurements were performed using digital images analyzed with ImageJ software.

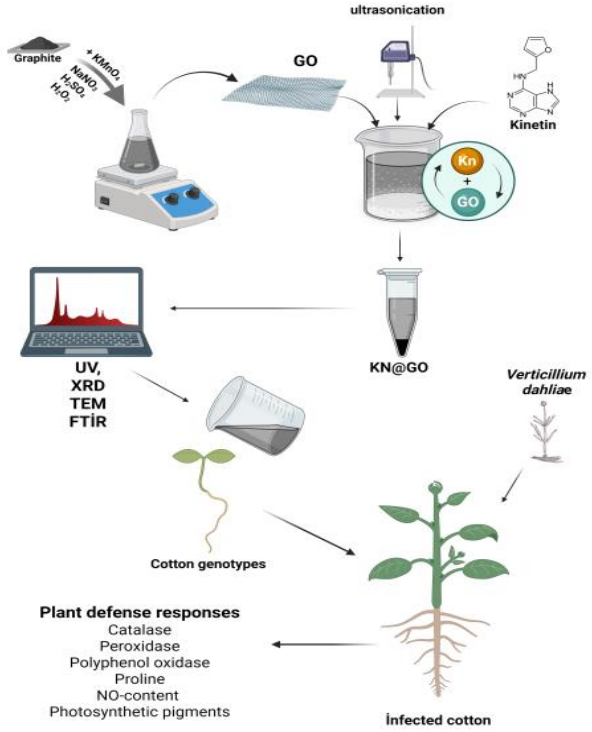

Fig. 6. Schematic representation of the experimental design

The development and biochemical parameters of the plants were determined at the 8th week of plant development.

Catalase (CAT) activity was determined using the gasometric method described by Mosheva (1982), based on measuring the volume of oxygen released during the decomposition of H_2O_2 by catalase. One gram of fresh plant tissue was homogenized in a porcelain mortar with glass fragments in distilled water (5 ml). To maintain a weakly alkaline medium (pH 6.9–7.7), optimal for catalase activity, 0.25 g of $CaCO_3$ was added to the homogenate. The final volume of the mixture was adjusted to 15 mL with distilled water.

The obtained homogenate was transferred into the reaction flask of a gasometric apparatus. Five milliliters of 3% H_2O_2 solution were placed into the side compartment of the system. After hermetic sealing of the apparatus, the reaction was initiated by mixing hydrogen peroxide with the homogenate. The reaction was carried out under continuous stirring using a magnetic stirrer at room temperature (22–25 °C) for 2 min.

Catalase activity was evaluated based on the volume of released oxygen, determined by changes in the water level in the burette of the gasometric system, and expressed as mL of O_2 $s^{-1} \bullet g^{-1}$ fresh weight.

Catalase activity was calculated using the following equation:

$$A_{CAT} = \frac{V}{t \times P}$$

where: A_{CAT} – catalase activity; V – volume of released oxygen (mL); t – reaction time (s); P – mass of plant material (g).

Guaiacol peroxidase (GPX, EC 1.11.1.7) activity was determined spectrophotometrically according to the method of Chance and Maehly (1955), based on the oxidation of guaiacol in the presence of H_2O_2. For the analysis, 100 mg of fresh plant tissue was homogenized in 5 mL of 0.06 M potassium phosphate buffer (pH 6.7), and the volume was adjusted to 25 mL with the same buffer. The extract was incubated for 15 min at room temperature and filtered through paper filter.

The reaction mixture contained 1 mL of enzyme extract, 1 mL of 0.06 M potassium phosphate buffer (pH 6.7), 1 mL of 2.38 mM guaiacol, and 1 mL of 0.1% H_2O_2. Changes in the absorbance were recorded at 440 nm using a Jenway 6850 UV/Vis spectrophotometer (Bibby Scientific Ltd., Staffordshire, UK, 2019) for 2.5 min at intervals of 10–15 s.

Enzyme activity was expressed as the change in absorbance at 440 nm per gram of fresh weight per minute ($\Delta A440\ g^{-1}\ FW\ min^{-1}$).

Polyphenol oxidase (PPO, EC 1.10.3.1) activity was determined according to the method of Ermakov et al. (1987), based on the oxidation of catechol in 0.1 M potassium phosphate buffer (pH 7.2). Fresh plant tissue (100 mg) was homogenized in phosphate buffer and filtered through paper filter to obtain the enzyme extract. The reaction mixture contained enzyme extract and 0.05 M catechol as a substrate. Changes in the absorbance were recorded at 590 nm using the Jenway 6850 UV/Vis spectrophotometer (Bibby Scientific Ltd., Staffordshire, UK, 2019). Enzyme activity was expressed as $\Delta A590\ g^{-1}\ FW\ min^{-1}$.

Nitric oxide (NO) content in plant tissues was determined using a modified method of Zhou et al. (2005), based on the conversion of endogenous NO into nitrite, followed by detection with Griess reagent. Fresh plant tissue (2 g) was homogenized on ice in 10 mL of 50 mM acetate buffer (pH 3.6) containing 2% zinc diacetate. The homogenate was centrifuged at 8,000 × g for 15 min at 4 °C. Subsequently, 250 mg activated charcoal was added to 10 mL of the supernatant, followed by filtration through paper filter.

For NO determination, 2 mL of filtrate was mixed with 1 mL of 1% Griess reagent, prepared in 12% acetic acid, and incubated for 30 min at room temperature in darkness. Absorbance was measured at 548 nm using the Jenway 6850 UV/Vis spectrophotometer (Bibby Scientific Ltd., Staffordshire, UK, 2019).

Nitrite concentrations were quantified using a $NaNO_2$ standard calibration curve, and NO content was calculated accordingly. Results were expressed as $\mu mol\ NO_2^-\ g^{-1}$ fresh weight.

Photosynthetic pigments (chlorophyll *a*, chlorophyll *b*, and carotenoids) were determined according to Wellburn and Lichtenthaler (1984). In summary, 1 g of fresh leaf tissue was homogenized in 20 mL of 80% acetone, followed by filtration, and absorbance was recorded at 440, 644, and 662 nm. Pigment concentrations were expressed as mg/g fresh weight.

Proline content was semiquantitatively analyzed using thin-layer chromatography (TLC) based on the modified method of Boctor (1971). Approximately 100 mg of fresh plant tissue was homogenized in 20% ethanol (10 µL/mg fresh weight) and centrifuged at 14,000 × g for 5 min at room temperature. Then, 10 µL of the supernatant was applied onto isatin-impregnated Whatman 3MM chromatography paper and air-dried for 30 min. Color development was performed by incubating the paper at 90 °C for 20 min. The intensity of the blue proline-isatin complex was recorded by digital imaging and analyzed using ImageJ software (National Institutes of Health, Bethesda, MD, USA). Proline accumulation was expressed as integrated density values (pixels) obtained from ImageJ analysis. All measurements were performed in three biological and three technical replicates.

Statistical analysis was performed using GraphPad Prism 10.4.0 (GraphPad Software, San Diego, CA, USA, 2024). Morphometric parameters, antioxidant enzyme activities (CAT, GPX and PPO), nitric oxide (NO) content, and photosynthetic pigment levels were analyzed using two-way ANOVA (Tukey's post-hoc test). The proline contents for genotypes were calculated using one-way ANOVA (Tukey's post-hoc test). Differences were considered statistically significant at $P < 0.05$. All biochemical measurements were performed in three biological and three technical replicates.

Results

The study included five treatment groups: control (*Gossypium hirsutum* L. TM-1 and *Gossypium barbadense* L. Pima 3-79), pathogen-infected TM-1 and Pima 3-79 plants, kinetin treated genotypes (both control and infected), and KN+GO treated genotypes (both control and infected). Based on generalized morphological observations of plant growth across the varieties, kinetin treatment significantly enhanced the growth of both TM-1 and Pima 3-79 plants, while the KN+GO nanoensemble further amplified this growth stimulation (Fig. 7).

According to the collected data, both TM-1 and Pima genotypes exhibited high germination rates (Table 1). However, a significant reduction in the survival rates was observed in both genotypes following pathogen exposure, indicating the high virulence of *Verticillium dahliae*. Notably, a twofold decrease in the seedling survival was recorded for the Pima genotype during pathogen stress, suggesting its greater susceptibility to infection compared with TM-1.

Table 1
Germination parameters of infected cotton genotypes under kinetin and KN+GO treatments (x ± SD, n = 3 independent experiments, 30 plants each)

Samples	Number of surviving plants	Percentage of surviving plants, %
TM-1 – Control	27 ± 1	90.0 ± 3.3^a
TM-1 – Control+pathogen	20 ± 2	66.7 ± 6.6^b
TM-1 – 10 µM kinetin	29 ± 1	96.7 ± 3.3^a
TM-1 – 10 µM kinetin + pathogen	26 ± 1	86.7 ± 3.3^a
TM-1 – 10 µM KN+GO	26 ± 1	86.7 ± 3.3^a
TM-1 – 10 µM KN+GO+pathogen	28 ± 1	93.3 ± 3.3^a
Pima – Control	28 ± 1	93.3 ± 3.3^a
Pima – Control+pathogen	14 ± 2	46.7 ± 6.6^c
Pima – 10 µM kinetin	22 ± 1	73.3 ± 3.3^{ab}
Pima – 10 µM kinetin+pathogen	22 ± 2	73.3 ± 6.6^{ab}
Pima – 10 µM KN+GO	28 ± 1	93.3 ± 3.3^a
Pima – 10 µM KN+GO+pathogen	26 ± 1	86.7 ± 3.3^a

Note: different letters indicate statistically significant differences between groups (one-way ANOVA followed by Tukey's post-hoc test, $P < 0.05$).

In the infected TM-1 seedlings treated with kinetin, the germination rate increased by 20%, compared with the plants subjected to pathogen infection. These findings suggest that kinetin application enhances resistance to pathogen stress in the TM-1 genotype. This protective effect may be associated with the activation of defense-related mechanisms or a direct inhibitory effect of kinetin on the pathogen.

Kinetin did not have a positive effect on the survival of the Pima plants compared with the control, leading to a 20% decrease. However, the results also showed that when kinetin was applied to the pathogen-infected Pima plants, their survival rate increased by 26.6% compared with the infected plants.

In the TM-1 genotype exposed to the KN+GO nanoensemble, no notable difference was observed compared with the control and pure kinetin treatments. However, in the pathogen-infected TM-1 plants treated with KN+GO, a 26.6% increase in the survival rate was recorded. This indicates that the nanoensemble specifically enhances the resistance to the pathogen and induces seedling germination.

Analyses carried out on the pathogen-infected Pima genotype revealed that the KN+GO nanoensemble led to a 40% increase in the percentage of surviving plants, whereas pure kinetin effect was not excessively pronounced.

Table 2
Morphometric parameters of pathogen infected cotton genotypes under kinetin and KN+GO treatments (x ± SD, n = 3 independent experiments, 10 plants each)

Samples	Stem length, cm	Root length, cm
TM-1 – Control	11.04 ± 0.36^a	8.61 ± 1.05^a
TM-1 – Control+pathogen	8.73 ± 0.15^b	12.49 ± 1.86^b
TM-1 – 10 µM kinetin	11.52 ± 0.64^a	11.23 ± 0.56^b
TM-1 – 10 µM kinetin+pathogen	9.13 ± 0.59^{ab}	7.41 ± 0.95^a
TM-1 – 10 µM KN+GO	11.30 ± 0.33^a	8.89 ± 2.15^a
TM-1 – 10 µM KN+GO+pathogen	9.28 ± 0.51^{ab}	9.93 ± 3.52^a
Pima – Control	13.97 ± 1.23^{ab}	11.94 ± 0.56^b
Pima – Control+pathogen	14.27 ± 0.77^{ab}	11.87 ± 1.43^b
Pima – 10 µM kinetin	13.87 ± 1.27^{ab}	10.65 ± 0.54^{ab}
Pima – 10 µM kinetin+pathogen	15.03 ± 0.26^c	14.54 ± 1.92^c
Pima – 10 µM KN+GO	12.89 ± 0.61^{ab}	14.67 ± 2.25^c
Pima – 10 µM KN+GO+pathogen	12.31 ± 1.39^{ab}	11.72 ± 2.31^b

Note: see Table 1.

According to the data presented in Table 2, the infection caused a noticeable decrease in the stem length and a simultaneous increase in the root length in the TM-1 genotype, both under normal conditions and upon exposure to the KN+GO nanoensemble, reflecting a stress-induced redistribution of resources toward the root system to enhance

water and nutrient uptake. Kinetin treatment slightly stimulated the stem elongation and root growth under normal conditions, confirming its growth-promoting role. However, this positive effect was significantly weakened during pathogen stress. In contrast to TM-1, the Pima genotype exhibited a higher resistance to the pathogen, with the stem and root lengths remaining largely unchanged under infection. Treatment with kinetin and KN+GO caused only minor changes in the Pima plants, indicating the presence of a genotype-specific resistance mechanism and reduced hormonal sensitivity under stress conditions.

Fig. 7. Different variations of *Gossypium hirsutum* L. TM-1 (*a*) and *Gossypium barbadense* L. Pima 3-79 (*b*) plants: control (*1*); pathogen (*2*); 10 µM kinetin (*3*); 10 µM kinetin+pathogen (*4*); 10 µM KN+GO (*5*); 10 µM KN+GO+pathogen (*6*)

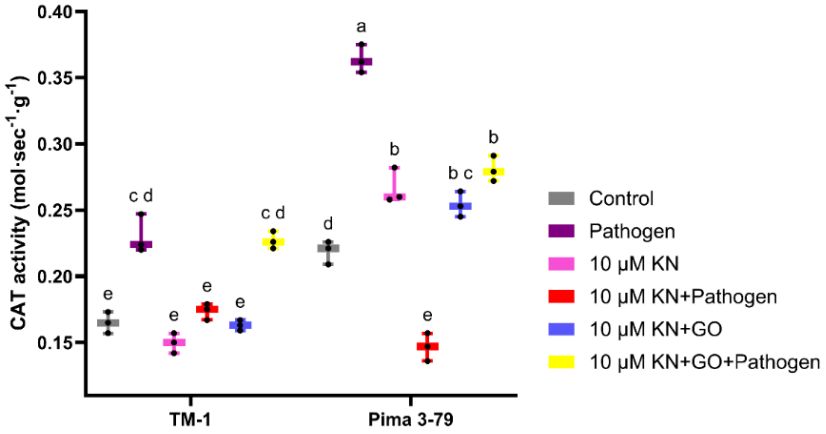

Fig. 8. Catalase activity in the leaves of *Gossypium hirsutum* L. TM-1 and *Gossypium barbadense* L. Pima 3-79 cotton genotypes under different treatements: different superscript letters indicate statistically significant differences between groups (two-way ANOVA followed by Tukey's post-hoc test, $P < 0.05$; $n = 3$)

The fungal infection significantly increased the catalase (CAT) activity in both TM-1 and Pima 3-79 genotypes compared with the control (Fig. 8), indicating the induction of oxidative stress. In TM-1, kinetin treatment alone did not cause significant changes in the CAT activity relative to the control, whereas in Pima 3-79, kinetin induced a slight increase in CAT activity, suggesting higher hormonal sensitivity of this genotype.

In the plants treated with kinetin and exposed to pathogen, the catalase activity (CAT) decreased in both TM-1 and Pima 3-79 genotypes compared with the control and kinetin-only treatments. This reduction was more pronounced in Pima 3-79, indicating genotype-dependent differences in antioxidant responses under pathogenesis.

Application of the KN+GO nanoensemble to the noninfected TM-1 plants did not significantly affect the CAT activity; however, under pathogen stress, the CAT activity increased markedly, reaching approximately 30% above the control levels. In Pima 3-79, the KN+GO nanoensemble caused only a slight increase in the CAT activity, and subsequent pathogen infection led to a moderate increase of approximately 13%, reflecting a weaker nanoensemble–pathogen interaction compared with TM-1.

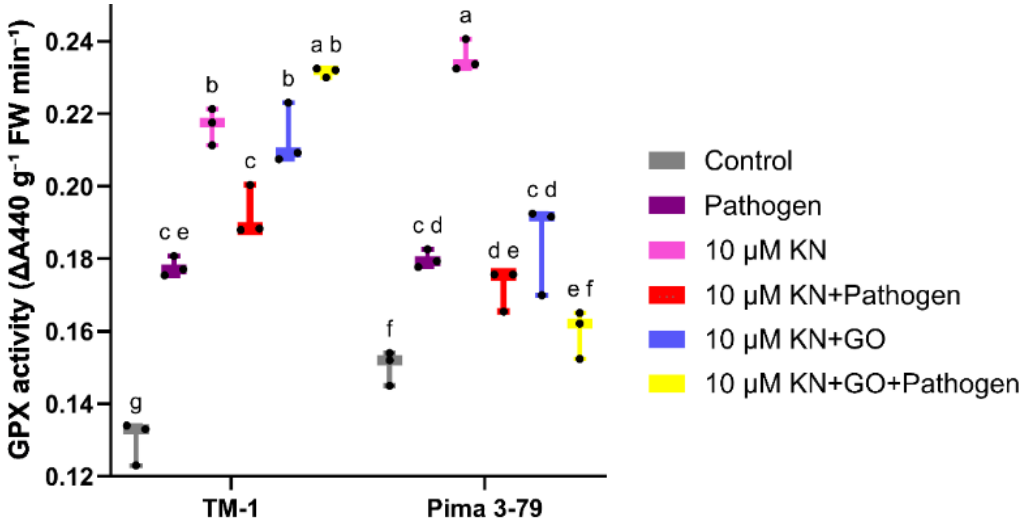

Fig. 9. Peroxidase activity in the leaves of cotton genotypes *Gossypium hirsutum* L. TM-1 and *Gossypium barbadense* L. Pima 3-79 under different treatements; different superscript letters indicate statistically significant differences between groups (two-way ANOVA followed by Tukey's post-hoc test, $P < 0.05$; $n = 3$)

As shown in Figure 9, the fungal infection decreased the peroxidase activity in both genotypes, measuring 15% in TM-1 and 10% in Pima 3-79, compared with the control. Kinetin treatment caused no statistically significant changes in the peroxidase activity in TM-1, whereas in Pima 3-79 the enzyme activity increased by 20%. In the plants treated with kinetin and exposed to pathogen, the peroxidase activity in both genotypes decreased again, approaching the values characteristic of the group with only exposure to pathogen.

The response to treatment with the KN+GO nanoensemble was genotype-specific. In the infected TM-1 plants, application of the nanoensemble led to an increase in the peroxidase activity, whereas in the infected Pima 3-79 genotype, further suppression of the enzyme activity was observed.

In the present study, despite a slight decrease in the polyphenol oxidase (PPO) activity in the pathogen-infected TM-1 variant (indicating an inhibitory effect of the pathogen on the defense system), no statistically significant changes in the enzyme activity were observed in the treatments with kinetin or the KN+GO nanoensemble. Similarly, in the Pima 3-79 genotype, both under healthy and pathogen-infected conditions, neither kinetin nor its nanoensemble altered the PPO activity (Fig. 10).

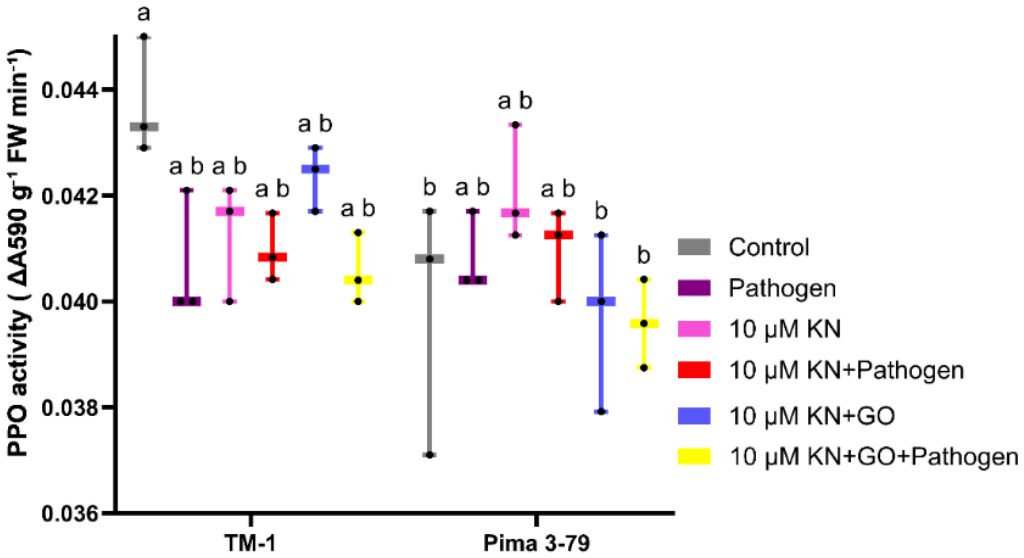

Fig. 10. Polyphenol oxidase activity in the leaves of *Gossypium hirsutum* L. TM-1 and *Gossypium barbadense* L. Pima 3-79 cotton genotypes under different treatements; different superscript letters indicate statistically significant differences between groups (two-way ANOVA followed by Tukey's post-hoc test, $P < 0.05$; $n = 3$)

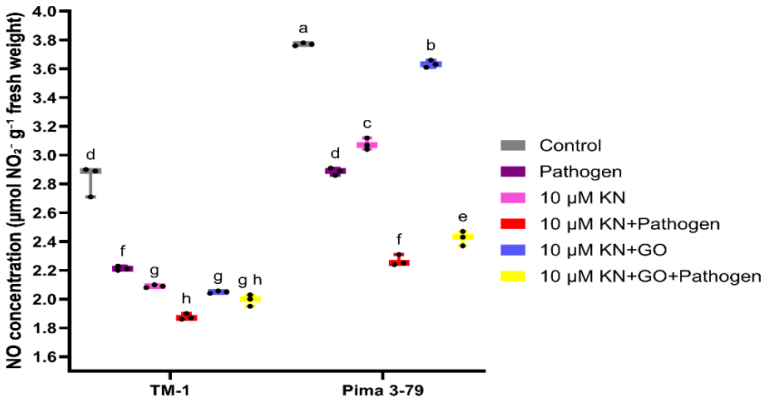

Fig. 11. Nitric oxide (NO) levels in the leaves of *Gossypium hirsutum* L. TM-1 and *Gossypium barbadense* L. Pima 3-79 cotton genotypes under different treatements: different superscript letters indicate statistically significant differences between groups (two-way ANOVA followed by Tukey's post-hoc test, $P < 0.05$)

In the present study, infection with *Verticillium dahliae* resulted in a significant reduction in the NO levels in both genotypes (Fig. 11). At the same time, neither kinetin nor the KN+GO nanoensemble promoted an increase in the NO levels. The combined action of the phytohormone and the pathogen did not lead to an additional significant decrease in the NO content. Taken together, these findings suggest that neither kinetin nor its graphene oxide-based nanoensemble participates in the induction of NO synthesis.

In the TM-1 genotype, pathogen exposure caused a pronounced increase in the content of all photosynthetic pigments compared with the control: Chlorophylls *a* and *b* increased by 70%, while carotenoids increased by 124% (Fig. 12a). Kinetin treatment resulted in a moderate elevation of the pigment levels (17–20%), whereas the combined application of the pathogen and kinetin led to a more substantial accumulation of pigments: Chlorophyll *a* increased by 71%, chlorophyll *b* by 92%, and carotenoids by 62% relative to the control. Application of the KN+GO nanoensemble also stimulated the pigment accumulation, and in the pathogen-infected TM-1 plants this effect was further enhanced, reaching 54–87% compared with the control.

In the Pima 3-79 genotype, pathogen treatment likewise induced increases in the content of photosynthetic pigments, although to a lesser extent: Chlorophyll *a* by 19%, chlorophyll *b* by 4%, and carotenoids by 36% (Fig. 12b). In contrast to TM-1, kinetin application in Pima 3-79 resulted in a slight reduction in the chlorophyll content (by 6%), and no significant changes were observed in the pathogen-infected plants. The KN+GO nanoensemble increased the chlorophyll *a* and *b* levels in the intact Pima 3-79 plants; however, this effect was not observed in the presence of the pathogen. In the TM-1 genotype, pathogen exposure led to a reduction in the proline levels compared with the control, as reflected by a decrease in the integrated pixel density (Fig. 13). Kinetin treatment caused an additional, though moderate, decrease in the proline content, and this effect was further intensified under combined kinetin and pathogen exposure. By contrast, application of the KN+GO nanoensemble resulted in a 9% increase in the proline levels, while the pathogen-infected plants treated with KN+GO exhibited a pronounced accumulation of proline, reaching 0.2 mM, which substantially exceeded the levels observed in all other treatments.

In the Pima 3-79 genotype, pathogen exposure also resulted in a significant reduction in the proline content. Kinetin application reduced the proline levels to below 0.1 mM; however, in the plants treated with kinetin and exposed to pathogen, the proline content increased relative to the kinetin-only variant. In the plants treated with the KN+GO nanoensemble, both in the absence and presence of the pathogen, no significant changes in the proline levels were observed, and the concentrations remained close to 0.1 mM.

Discussion

Based on previous data, external stress factors negatively affect cotton growth and development, reducing its yield and causing pathologies at the morphophysiological and biochemical levels. One of the primary pests of cotton is the pathogenic fungus *Verticillium dahliae*. Due to its high virulence and rapid spread under favorable conditions, this pathogen causes severe damage to cotton, posing a significant threat to cotton fields even in developed countries such as China, Australia, and the USA (Dadd-Daigle et al., 2021).

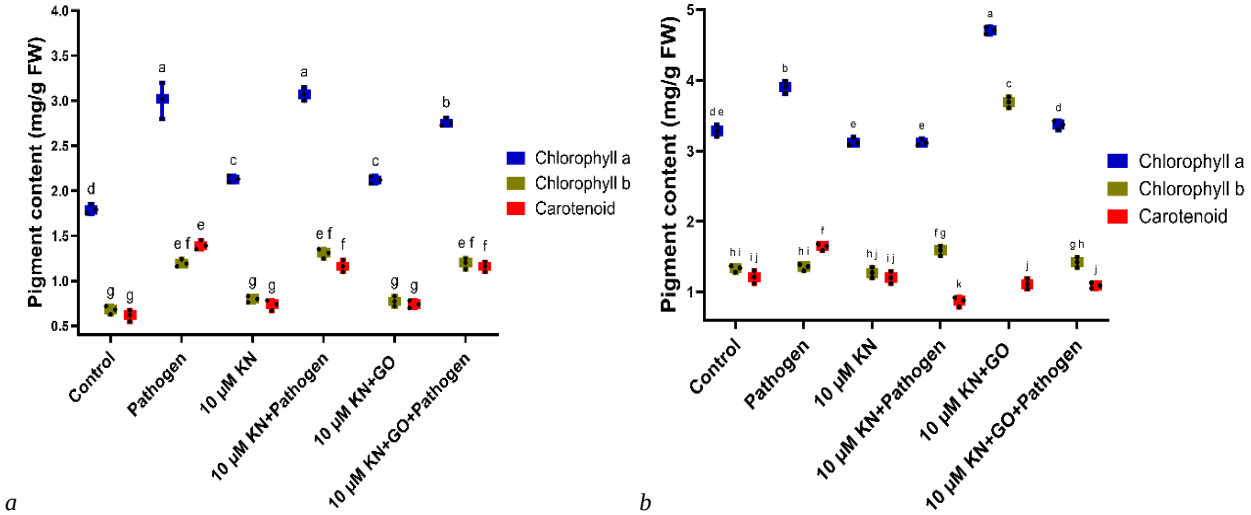

Fig. 12. The amounts of chlorophyll *a*, *b*, and carotenoids in the leaves of *Gossypium hirsutum* L. TM-1 (*a*) and *Gossypium barbadense* L. Pima 3-79 (*b*) cotton genotypes under different treatements: different superscript letters indicate statistically significant differences between groups (two-way ANOVA followed by Tukey's post-hoc test, $P < 0.05$; $n = 3$)

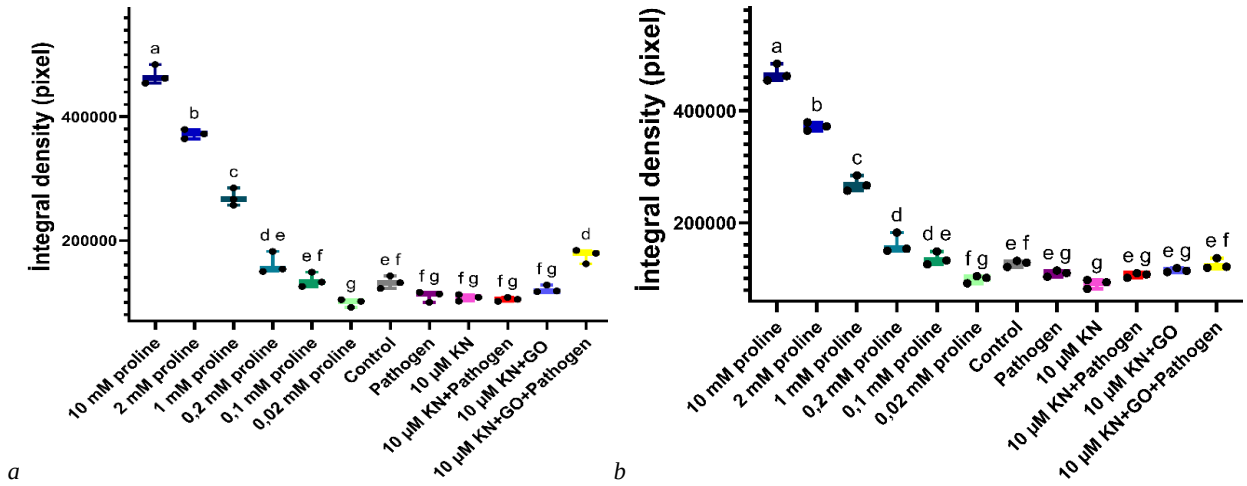

Fig. 13. Densitometric analysis results of proline determination in the leaves of *Gossypium hirsutum* TM-1 (*a*) and *Gossypium barbadense* Pima 3-79 (*b*) cotton genotypes using ImageJ software: different superscript letters indicate statistically significant differences between groups (one-way ANOVA followed by Tukey's post-hoc test, $P < 0.05$; $n = 3$)

The negative impact of this pathogen on cotton yield, along with the global population increase and rising demand for fiber and oilseed crops, has underscored the need for measures to prevent its spread (Maryum et al., 2022). Previous research has shown that the initial contact of the pathogen with the plant occurs in the early growth stages, specifically during germination. During this phase, the pathogen infects the roots and subsequently enters the xylem tissue, eventually causing wilting in the plant (Zhang et al., 2016).

To prevent the harmful effects of the pathogen, one possible approach is to enhance the plant's immune response by utilizing its natural defense potential, which includes the incorporation of phytoinducers (phytohormones or their derivatives) into this process (Gao et al., 2013). Considering the negative effects of pathogens on plant germination (Hersh et al., 2012), our experiment demonstrated a significant reduction in seed germination in both genotypes. However, in the TM-1 genotype, treated with both kinetin and KN+GO, the plant's survival ability under pathogen stress increased, which may indicate an enhancement of biochemical resistance mechanisms against the pathogen.

Interestingly, in the Pima 3-79 genotype, the KN+GO treatment had significant effects on the plant survival both under normal conditions and during pathogen exposure. This effect was stronger than in the plants treated with kinetin alone. These results suggest that the Pima 3-79 genotype is more sensitive to graphene oxide, while the TM-1 genotype exhibits higher sensitivity to kinetin.

Recent studies have shown that carbon-based nanostructures have a significant effect on plant development (Fernández-Gómez et al., 2023). Our results suggest that although kinetin and KN+GO enhance growth and partially alleviate the inhibitory effect of the pathogen in TM-1, the Pima genotype is characterized by distinct adaptive stability against the pathogen and a limited response to exogenous treatment with the phytohormone and its nanoensemble.

When comparing the growth intensities of the plants by examining root and stem lengths, it was found that the pathogen negatively affected the growth of the TM-1 plants, slowing stem growth and stimulating root development. Free kinetin stimulated stem growth, but its effectiveness may have decreased under the stress conditions caused by the pathogen. This phenomenon may be associated with pathogen-induced impairment of water and mineral transport through the xylem vessels (Yadeta & Thomma, 2013).

The response of the Pima genotype to the pathogen, kinetin, and KN+GO was different from that of the TM-1 genotype. The pathogen generally had minimal impact on the growth of the stems and roots of the Pima plants, which may be explained by the onset of individual resistance to the pathogen at a later developmental stage. Similarly, kinetin did not stimulate the growth in the Pima genotype.

The observed increase in catalase activity in both genotypes following pathogen infection confirms that the pathogen induces oxidative stress, thereby activating antioxidant defense mechanisms. Such responses are characteristic of plant–pathogen interactions, in which excessive production of reactive oxygen species (ROS) serves as an early defense signal but requires strict regulation to prevent cellular damage (Amil-Ruiz et al., 2011; Camejo et al., 2016).

Genotype-specific differences in CAT regulation suggest distinct strategies for maintaining redox homeostasis. The higher sensitivity of Pima 3-79 to kinetin under unstressed conditions indicates enhanced hormonal responsiveness; however, under pathogen stress, kinetin failed to sustain CAT activation and even reduced the enzyme activity relative to the pathogen-only treatments. This suggests that cytokinin signaling pathways may be suppressed or reprogrammed during pathogenesis. By contrast, the KN+GO nanoensemble markedly enhanced the CAT activity in the pathogen-infected TM-1 plants, indicating its potential to reinforce antioxidant defenses under stress conditions. The weaker induction of CAT observed in Pima 3-79 may reflect not a reduced defense capacity, but rather a lower degree of pathogen-induced oxidative stress. It is assumed that this genotype possesses more effective basal or genotype-specific resistance mechanisms that limit the impact of the pathogen, thereby reducing the need for a pronounced CAT-dependent antioxidant response.

Overall, these findings demonstrate that graphene oxide-based nanoensembles can modulate plant antioxidant responses in a genotype- and stress-dependent manner.

The decrease in peroxidase activity under pathogen exposure is consistent with reports describing suppression of the plant antioxidant system during pathogenesis, which can lead to impairment of protective mechanisms (Kużniak & Skłodowska, 2005). Such suppression is often associated with prolonged and intensive pathogen effects on key components of antioxidant defense.

Previous studies have shown that in wheat plants infected with *Septoria nodorum*, an initial decrease in peroxidase activity was accompanied by the accumulation of hydrogen peroxide, enhancing oxidative pressure against the pathogen (Yusupova et al., 2006). The results obtained in the present study likewise indicate pathogen-induced suppression of peroxidase activity in both cotton genotypes.

Differences in responses to kinetin and the KN+GO nanoensemble indicate genotype-specific features of peroxidase activity regulation. In the TM-1 genotype, relative stability of the enzymatic response was observed, and during pathogen stress the KN+GO nanoensemble promoted an increase in peroxidase activity, which may indicate a stabilizing effect of the phytohormone in nanoform. By contrast, in the Pima 3-79 genotype, both kinetin and KN+GO caused more pronounced changes in peroxidase activity, reflecting increased sensitivity of this genotype to hormonal and nano-induced effects.

Polyphenol oxidase plays an important role in plant defense responses, particularly through the synthesis of quinones. The active involvement of PPO in plant defense against pathogens and the positive correlation between increased PPO activity and enhanced resistance

have been demonstrated in several studies (Mayer, 2006; Zhang et al., 2021). Polyphenol oxidase participates in plant defense reactions, including activation of leucine-rich repeat receptor-like protein kinases, reinforcement of antioxidant defenses, and performance of cytotoxic activity against bacterial pathogens. Disruption of PPO synthesis is therefore considered a critical factor influencing the effectiveness of plant defense responses (Ryan et al., 2014; Laohavisit et al., 2020).

The absence of significant changes in the polyphenol oxidase activity supports the notion that defense responses induced by kinetin and the KN+GO nanoensemble are primarily associated with redox regulation rather than with phenolic oxidation pathways.

Cytokinins are known to function as scavengers of nitric oxide, acting as dynamic suppressors of NO accumulation. Given that NO serves as a secondary signaling messenger in plant defense responses, the mechanisms by which cytokinin-pathogen interactions influence NO levels and, consequently, cotton resistance remains insufficiently understood (Liu et al., 2013; Lutter et al., 2024). In its free radical form, NO regulates a wide range of plant developmental processes, including seed germination, root growth, flowering, and fruit development, and plays a key role in the activation of defense responses against abiotic and biotic stresses, including fungal and bacterial pathogens (Trapet et al., 2015; Martínez-Medina et al., 2019; Rashid et al., 2021). In the present study, infection with *Verticillium dahliae* resulted in a significant reduction in NO levels in both genotypes, whereas neither kinetin nor the KN+GO nanoensemble, in combination with the pathogen, induced NO accumulation.This effect may be associated with pathogen-mediated suppression of hypersensitive responses in plants (Bellin et al., 2013).

Overall, pathogen exposure led to an increase in photosynthetic pigment content in both genotypes, which may reflect a stress-induced adaptive response. The effects of kinetin and its nanoensemble were strongly genotype-dependent: TM-1 exhibited stimulation of the photosynthetic apparatus, particularly under pathogen stress, whereas in Pima 3-79 this effect was attenuated or absent. This indicates differences in the regulation of the photosynthetic machinery and in the sensitivity to phytohormonal treatments between the genotypes.

Photosynthesis plays a crucial role in the development of energy resources that support plant tolerance to adverse environmental conditions (Nawaz et al., 2023). Despite reports of suppressed photosynthetic activity following infection with biotrophic pathogens (Chou et al., 2000), the results of the present study suggest that, in the examined genotypes, increased accumulation of photosynthetic pigments may represent a component of a defensive strategy aimed at maintaining metabolic activity under stress conditions.

Proline is an important component of plant defense responses to abiotic and biotic stresses. It is well established that upon initial pathogen contact, proline catabolism is activated, leading to the formation of pyrroline-5-carboxylate, a signaling metabolite associated with the induction of hypersensitive responses and the generation of reactive oxygen species (ROS) (Maxwell & Davis, 2000; Lee et al., 2013). In the present study, the reduction in the proline levels in TM-1 following pathogen and kinetin treatment may indicate suppression of proline-mediated defense mechanisms. By contrast, the pronounced accumulation of proline observed in the KN+GO- and pathogen-treated plants likely reflects activation of antioxidant defense pathways, coordinated with catalase and peroxidase activity, thereby contributing to the prevention of cell death.

The increase in the proline levels under KN+GO treatment in the presence of pathogen stress, observed in both genotypes, suggests a potential synergistic interaction between the phytohormone and the nanomaterial and indicates the involvement of similar defense mechanisms in TM-1 and Pima 3-79 (Camejo et al., 2016).

In summary, nanoensemble KN+GO was synthesized via non-covalent interactions. The structure and morphology were characterized by transmission electron microscopy (TEM), FTIR spectroscopy, and powder X-ray diffraction (XRD), confirming successful immobilization of kinetin on the graphene oxide via hydrogen bonds and π–π interactions. The loading of kinetin onto GO was determined by UV–Vis spectroscopy. The nanoensemble KN+GO exerted a pronounced effect on the growth of individual plant organs and seed germination. Compared with pure kinetin, the KN+GO nanoensemble more effectively enhanced plant survival, stabilized growth parameters, and modulated key components of the antioxidant defense system during *Verticillium dahliae* infection. In particular, the enhancement of catalase activity under pathogen-induced stress (especially in susceptible genotypes) highlights the role of KN+GO nanoensembles in strengthening redox homeostasis and stress tolerance.

Genotype-dependent differences between TM-1 and Pima 3-79 reflect distinct adaptive strategies and sensitivities to phytohormonal and nano-enabled treatments. While Pima 3-79 exhibited inherent tolerance to pathogen stress, the KN+GO nanoensemble contributed to improved redox regulation and maintenance of physiological stability without excessive activation of defense signaling pathways.

Conclusion

In the present study, nanoensemble KN+GO was synthesized via non-covalent interactions. The structure and morphology were characterized by transmission electron microscopy (TEM), FTIR spectroscopy, and powder X-ray diffraction (XRD), confirming successful immobilization of kinetin on the graphene oxide GO via hydrogen bonds and π–π interactions. The loading of kinetin on GO was determined using UV-Vis spectroscopy. The nanoensemble KN+GO was shown to exert a pronounced effect on the growth of individual plant organs and seed germination. Compared with pure kinetin, the KN+GO nanoensemble more effectively enhanced the plant survival, stabilized the growth parameters, and modulated key components of the antioxidant defense system under *Verticillium dahliae* infection. In particular, the enhancement of catalase activity under pathogen-induced stress highlights the role of KN+GO nanoensembles in strengthening redox homeostasis and stress tolerance. The increase in the proline content observed in the pathogen-treated variants supplemented with KN+GO indicates that GO-based nanoensemble treatments promote proline synthesis, thereby contributing to enhanced stress adaptation.

This work was performed in collaboration with Baku State University and the Hebrew University of Jerusalem.

References

Ahmadov, I. S., Ramazanov, M. A., Gasimov, E. K., Rzayev, F. H., & Veliyeva, S. B. (2020).The migration study of nanoparticles from soil to the leaves of plants. Biointerface Research in Applied Chemistry, 10(5), 6101–6111.

Alizada, S., Aliyeva, K., Mammadova, R., Bayramli, O., & Moghanloo, B. S. (2024). Salinity, *Verticillium* wilt tolerance and genetic diversity analysis of upland cotton genotypes. Advances in Biology and Earth Sciences, 9(2), 242–252.

Amil-Ruiz, F., Blanco-Portales, R., Munoz-Blanco, J., & Caballero, J. L. (2011). The strawberry plant defense mechanism: A molecular review. Plant and Cell Physiology, 52(11), 1873–1903.

Baghirov, M. B., Muradov, M., Eyvazova, G., Mammadyarova, S., Gahramanli, L., Aliyeva, G., Huseynov, E., & Abdullayev, M. (2023). Features of structure and optical properties GO and a GO/PVA composite subjected to gamma irradiation. RSC Advances, 13(50), 35648–35658.

Barnaby, S. N., Frayne, S. H., Fath, K. R., & Banerjee, I. A. (2011). Growth of Se nanoparticles on kinetin assemblies and their biocompatibility studies. Soft Materials, 9(4), 313–334.

Bellin, D., Asai, S., Delledonne, M., & Yoshioka, H. (2013). Nitric oxide as a mediator for defense responses. Molecular Plant-Microbe Interactions, 26(3), 271–277.

Boctor, F. N. (1971). An improved method for colorimetric determination of proline with isatin. Analytical Biochemistry, 43(1), 66–70.

Camejo, D., Guzmán-Cedeño, Á., & Moreno, A. (2016). Reactive oxygen species, essential molecules, during plant–pathogen interactions. Plant Physiology and Biochemistry, 103, 10–23.

Chance, B., & Maehly, A. C. (1955). Assay of catalases and peroxidases. Methods of Biochemical Analysis, 1, 357–424.

Chen, J., Peng, H., Wang, X., Shao, F., Yuan, Z., & Han, H. (2014). Graphene oxide exhibits broad-spectrum antimicrobial activity against bacterial phytopathogens and fungal conidia by intertwining and membrane perturbation. Nanoscale, 6(3), 1879–1889.

Choi, J., Choi, D., Lee, S., Ryu, C. M., & Hwang, I. (2011). Cytokinins and plant immunity: Old foes or new friends? Trends in Plant Science,16(7), 388–394.

Chou, H. M., Bundock, N., Rolfe, S. A., & Scholes, J. D. (2000). Infection of *Arabidopsis thaliana* leaves with *Albugo candida* (white blister rust) causes a reprogramming of host metabolism. Molecular Plant Pathology, 1(2), 99–113.

Chun, J., Wan, M., Guo, H., Zhang, Q., Feng, Y., Tang, Y., Zhu, B., Sang, Y., Jing, S., Chen, T., & Zeng, Z. (2024). Cytokinin-mediated enhancement of potato growth and yield by *Verticillium dahliae* effector VDAL under low temperature stress. BMC Plant Biology, 24(1), 1115.

Dadd-Daigle, P., Kirkby, K., Chowdhury, P. R., Labbate, M., & Chapman, T. A. (2021). The *Verticillium* wilt problem in Australian cotton. Australasian Plant Pathology, 50(2), 129–135.

Di, X., Takken, F. L., & Tintor, N. (2016). How phytohormones shape interactions between plants and the soil-borne fungus *Fusarium oxysporum*. Frontiers in Plant Science, 7, 170.

Ermakov, A. I., Arasimovich, V. V., Yarosh, N. P., Peruanskiy, Y. V., Lukovnikova, G. A., & Ikonnikova, M. I. (1987). Methods of biochemical investigation of plants. Agropromizdat, Leningrad (in Russian).

Fatehi, S. F., Oraei, M., Gohari, G., Akbari, A., & Faramarzi, A. (2022). Proline-functionalized graphene oxide nanoparticles (GO–Pro NPs) mitigate salt-induced adverse effects on morpho-physiological traits and essential oils constituents in Moldavian balm (*Dracocephalum moldavica* L.). Journal of Plant Growth Regulation, 41(7), 2818–2832.

Fernández-Gómez, D., Villegas-Moreno, J., Kumar-Tiwari, D., Gómez-Romero, M., & Juárez-Cisneros, G. (2023). Effect of multi-walled carbon nanotubes functionalized with kinetin on the development of *Avena sativa*. Microscopy and Microanalysis: the Official Journal of Microscopy Society of America, Microbeam Analysis Society, Microscopical Society of Canada, 29(S1), 42–43.

Gao, W., Long, L., Zhu, L. F., Xu, L., Gao, W. H., Sun, L. Q., Liu, L. L., & Zhang, X. L. (2013). Proteomic and virus-induced gene silencing (VIGS) analyses reveal that gossypol, brassinosteroids, and jasmonic acid contribute to the resistance of cotton to *Verticillium dahliae*. Molecular and Cellular Proteomics, 12(12), 3690–3703.

Göre, M. E. (2007). Vegetative compatibility and pathogenicity of *Verticillium dahliae* isolates from the aegean region of Turkey. Phytoparasitica, 35(3), 222–231.

Hajiyeva, S., Hasanova, U., Gakhramanova, Z., Israyilova, A., Ganbarov, K., Gasimov, E., & Maharramov, A. (2019). The role of diazacrown ether in the enhancement of the biological activity of silver nanoparticles. Turkish Journal of Chemistry, 43(6), 1711–1721.

Hersh, M. H., Vilgalys, R., & Clark, J. S. (2012). Evaluating the impacts of multiple generalist fungal pathogens on temperate tree seedling survival. Ecology, 93(3), 511–520.

Hidayah, N. M. S., Liu, W. W., Lai, C. W., Noriman, N. Z., Khe, C. S., Hashim, U., & Lee, H. C. (2017). Comparison on graphite, graphene oxide and reduced graphene oxide: Synthesis and characterization. AIP Conference Proceedings, 1892(1), 150002.

Huseynzada, A., Hasanova, U., & Gakhramanova, Z. (2023). Graphene oxide-modified dihydropyrimidines. Azerbaijan Chemical Journal, 3, 142–151.

Joost, O., Bianchini, G., Bell, A. A., Benedict, C. R., & Magill, C. W. (1995). Differential induction of 3-hydroxy-3-methylglutaryl CoA reductase in two cotton species following inoculation with *Verticillium*. Molecular Plant-Microbe Interactions, 8(6), 880–885.

Kabiri, S., Degryse, F., Tran, D. N. H., da Silva, R. C., McLaughlin, M. J., & Losic, D. (2017). Graphene oxide: A new carrier for slow release of plant micronutrients. ACS Applied Materials and Interfaces, 9(49), 43325–43335.

Kalidas, N., Gopal, P. M., & Kavimani, V. (2025). Development and characterization of silicon nitride and synthesized graphene oxide reinforced Cu/GO/xSi_3N_4 composites. Silicon, 17(1), 141–153.

Kużniak, E., & Skłodowska, M. (2005). Fungal pathogen-induced changes in the antioxidant systems of leaf peroxisomes from infected tomato plants. Planta, 222(1), 192–200.

Laohavisit, A., Wakatake, T., Ishihama, N., Mulvey, H., Takizawa, K., Suzuki, T., & Shirasu, K. (2020). Quinone perception in plants via leucine-rich-repeat receptor-like kinases. Nature, 587(7832), 92–97.

Lee, I. R., Lui, E. Y., Chow, E. W., Arras, S. D., Morrow, C. A., & Fraser, J. A. (2013). Reactive oxygen species homeostasis and virulence of the fungal pathogen *Cryptococcus neoformans* requires an intact proline catabolism pathway. Genetics, 194(2), 421–433.

Liu, W. Z., Kong, D. D., Gu, X. X., Gao, H. B., Wang, J. Z., Xia, M., Gao, Q., Tian, L. L., Xu, Z. H., Bao, F., Hu, Y., Ye, N. S., Pei, Z. M., & He, Y. K. (2013). Cytokinins can act as suppressors of nitric oxide in *Arabidopsis*. Proceedings of the National Academy of Sciences, 110(4), 1548–1553.

Lutter, F., Brenner, W., Krajinski-Barth, F., & Safavi-Rizi, V. (2024). Nitric oxide and cytokinin cross-talk and their role in plant hypoxia response. Plant Signaling and Behavior, 19(1), 2329841

Magro, M. R., Vella, D. A., & Cassar, G. (2025). Synthesis of graphene oxide: A refined approach. Carbon Trends, 20, 100509.

Mammadova, R. B., Akparov, Z. I., Alızade, S. A., Amrahov, N. R., & Abdulalıyeva, G. S. (2025). *Verticillium* wilt effect on fiber production and its quality traits in upland cotton (*Gossypium hirsutum* L.). SABRAO Journal of Breeding and Genetics, 57(5), 2015–2023.

Martínez-Medina, A., Pescador, L., Terrón-Camero, L. C., Pozo, M. J., & Romero-Puertas, M. C. (2019). Nitric oxide in plant–fungal interactions. Journal of Experimental Botany, 70(17), 4489–4503.

Maryum, Z., Luqman, T., Nadeem, S., Khan, S. M. U. D., Wang, B., Ditta, A., & Khan, M. K. R. (2022). An overview of salinity stress, mechanism of salinity tolerance and strategies for its management in cotton. Frontiers in Plant Science, 13, 907937.

Maxwell, S. A., & Davis, G. E. (2000). Differential gene expression in p53-mediated apoptosis-resistant vs. apoptosis-sensitive tumor cell lines. Proceedings of the National Academy of Sciences, 97(24), 13009–13014.

Mayer, A. M. (2006). Polyphenol oxidases in plants and fungi: Going places? A review. Phytochemistry, 67(21), 2318–2331.

Nawaz, M., Sun, J., Shabbir, S., Khattak, W. A., Ren, G., Nie, X., Bo, Y., Javed, Q., Du, D., & Sonne, C. (2023). A review of plants strategies to resist biotic and abiotic environmental stressors. Science of the Total Environment, 900, 165832.

Park, S., Choi, K. S., Kim, S., Gwon, Y., & Kim, J. (2020). Graphene oxide-assisted promotion of plant growth and stability. Nanomaterials, 10(4), 758.

Rashid, A. N., Janda, M., Mahmud, M. Z., Valentová, O., Burketová, L., & Alekber, Q. A. (2021). Influence of salt stress on the Flg22-induced ROS production in *Arabidopsis thaliana* leaves. Pakistan Journal of Botany, 53(5), 1605–1610.

Ryan, A., Kaplan, E., Nebel, J. C., Polycarpou, E., Crescente, V., Lowe, E., Preston, G. M., & Sim, E. (2014). Identification of NAD(P)H quinone oxidoreductase activity in azoreductases from *P. aeruginosa*: Azoreductases and NAD(P)H quinone oxidoreductases belong to the same FMN-dependent superfamily of enzymes. PloS One, 9(6), e98551.

Taghiyeva, N., Hasanova, U., Millet, M., Gardiennet, C., Gakhramanova, Z., Mirzayev, M. H., Gahramanli, L., Pham-Huu, C., Aliyeva, S., Aliyeva, G., Rzayev, F., Gasimov, E., Boulogne, C., & Akhundzada, H. V. (2024). Synthesis and characterization of novel adsorbents based on functionalization of graphene oxide with Schiff base and reduced Schiff base for pesticide removal. Materials, 17(16), 4096.

Trapet, P., Kulik, A., Lamotte, O., Jeandroz, S., Bourque, S., Nicolas-Francès, V., Rosnoblet, C., Besson-Bard, A., & Wendehenne, D. (2015). NO signaling in plant immunity: a tale of messengers. Phytochemistry, 112, 72–79.

Wellburn, A. R., & Lichtenthaler, H. (1984). Formulae and program to determine total carotenoids and chlorophylls *a* and *b* of leaf extracts in different solvents. Advances in Photosynthesis Research, 2, 9–12.

Yadeta, K. A., & J. Thomma, B. P. (2013). The xylem as battleground for plant hosts and vascular wilt pathogens. Frontiers in Plant Science, 4, 97.

Yusupova, Z. R., Khairullin, R. M., & Maksimov, I. V. (2006). The activity of peroxidase in various cell fractions of wheat plants infected with *Septoria nodorum* berk. Russian Journal of Plant Physiology, 53(6), 807–813.

Zhang, T., Jin, Y., Zhao, J. H., Gao, F., Zhou, B. J., Fang, Y. Y., & Guo, H. S. (2016). Host-induced gene silencing of the target gene in fungal cells confers effective resistance to the cotton wilt disease pathogen *Verticillium dahliae*. Molecular Plant, 9(6), 939–942.

Zhang, Y., Zhu, H., Ye, Y., & Tang, C. (2021). Antifungal activity of chaetoviridin A from *Chaetomium globosum* CEF-082 metabolites against *Verticillium dahliae* in cotton. Molecular Plant-Microbe Interactions, 34(7), 758–769.

Zhou, B., Guo, Z., Xing, J., & Huang, B. (2005). Nitric oxide is involved in abscisic acid-induced antioxidant activities in *Stylosanthes guianensis*. Journal of Experimental Botany, 56(422), 3223–3228.

Zhu, Y., Zhao, M., Li, T., Wang, L., Liao, C., Liu, D., Zhang, H., Zhao, Y., Liu, L., Ge, X., & Li, B. (2023). Interactions between *Verticillium dahliae* and cotton: Pathogenic mechanism and cotton resistance mechanism to *Verticillium* wilt. Frontiers in Plant Science, 14, 1174281.